Fifth International Conference on CFD in the Process Industries
CSIRO, Melbourne, Australia
13-15 December 2006

MODELING OF SEPARATION OF METAL IONS IN A MICROFLUIDIC CHIP

Anh BUI, Yonggang ZHU and Karolina PETKOVIC-DURAN
CSIRO Microfluidics Laboratory
CSIRO Manufacturing & Materials Technology, Highett, Victoria 3190, AUSTRALIA
Yonggang.zhu@csiro.au

ABSTRACT

Numerical simulation of the separation of metal ions in a microfluidic cross-chip is presented. The models of electroosmotic flow and electrophoretic migration of charged particles resulted from the applied electrical field are developed and implemented in the CFX-4 CFD software. The models are shown to be able to describe the involved electro-chemical and physical processes happening in complex microfluidic chip geometry.

NOMENCLATURE

c	concentration, mol/m^3	α	degree of dissociation
D	diffusivity, m^2/s	ε	dielectric constant
F	Faraday constant, C/mol	ζ	zeta potential, V
R	gas constant, J/(mol.K)	μ	dynamic viscosity, Pa.s
$\mathbf{v}$	velocity, m/s	ρ	density, kg/m^3
i	subscript for ith ionic components	σ	electrical conductivity, S/m
		ϕ	electrical potential, V
		ω	mobility, m^2/(V.s)

INTRODUCTION

Over the last decade, microfluidic devices have been intensively developed and used for sampling, mixing, separation, sensing and miniaturised chemical and biological reaction platforms. By demonstrating radical reductions in size and weight, and better heat transfer, mass transfer and other performance advantages compared to conventional systems, microfluidic devices have the potential to revolutionize chemical analysis, chemical synthesis, industrial automation, plant safety, medical and biomedical applications.

Separation is one of the many important functions that a microfluidic chip may perform. One way of separating molecules is electrophoresis. The electrophoretic separation technique is based on the principle that, under the influence of an applied potential field, different species in solution will migrate at different velocities from one another. When an external electrical field is applied to a solution of charged species, each ion moves toward the electrode of opposite charge. Electrophoresis has been performed on a support medium that acts as physical support and mechanical stability for the fluidic buffer system. Capillary electrophoresis has emerged as an alternative format for medium-based ones and, with the advent of microtechnology, gained popularity in microchip applications.

Electrokinetically driven flow in microchannels is complex due to the interaction of surface-flow interaction, electrochemistry and multi-physics processes involved. While extensive experimental studies have been carried out in the field since the last two decades (e.g. Dolnik et al., 2000, Hu and Dovichi, 2002), computer simulations have played an important role in the study of the electrokinetically driven flows, including electrophoretic separation in microflows. This is mainly due to the capability in dealing simultaneously with many electro-chemical and physical processes involved in the electrophoresis. The previous works by various authors (see Ikuta et al. (1998), Ermakov et al. (1994, 1998, 2000), and Sounart et al. (2000, 2001)) indicate that the phenomena could be described in the framework of the conservation laws of mass and charge and by coupling of the involved electro-chemical kinetics and heat-mass transfer.

In the past, many numerical studies of electro-osmosis and electrophoresis have been limited by 1D approximation which could not correctly model the flow and particle migration in the complex geometry of a microfluidic cross-chip. Moreover, few studies have described the full coupling between the processes of ionic transport, electric field variation, and heat transfer, involved in the electrokinetically driven flow and particle migration.

The aim of this study is to develop a 3D computational model of electrokinetically driven (or electroosmotic) flow and electrophoretic separation and to validate using available experimental data obtained at the CSIRO microfluidic laboratory.

MODEL DESCRIPTION

The model consists of a system of differential equations describing the heat, mass, momentum, and ionic species conservations and constitutive dependencies.

Equations of mass conservation of ionic species

The mass conservation is given by the convective-diffusive equation, via,

$$\frac{\partial c_i}{\partial t} + \nabla \cdot (\vec{\mathrm{v}}_i c_i) = \nabla \cdot (D_i \nabla c_i) \,. \qquad (1)$$

Mobilities of solution and ionic species

The bulk buffer solution flow is driven by the electrokinetic force (osmotic flow) while the motion of the charged particles (ions) is governed by capillary electrophoresis. The velocity of the ions is given by,

$$\vec{v}_i = -(\omega_{eo} + \omega_{ep,i})\nabla\phi\,, \qquad (2)$$

where ω_{eo} and $\omega_{ep,i}$ are the effective electroosmotic mobility of the solution and electrophoretic mobility of i^{th} ionic species, respectively. The effective mobility of a charged particle which appears in the electrophoretic migration velocity is defined by

$$\omega_{ep,i} = \alpha_i \omega_{0,i} \qquad (3)$$

where α_i and $\omega_{0,i}$ is the degree of dissociation and mobility of i^{th} ionic species.

The electroosmotic mobility is defined as

$$\omega_{eo} = -\frac{\varepsilon\zeta}{\mu} \qquad . \qquad (4)$$

Diffusion coefficient

The diffusion coefficient is defined by Nernst-Einstein equation (e.g. Probstein, 2003),

$$D_i = \frac{RT\left|\omega_{ep,i}\right|}{F} \qquad (5)$$

The dependence of D_i on concentration is not considered here.

Electrical potential

The electrical field in the solution is described by (Probstein, 2003)

$$\nabla\cdot(\sigma\nabla\phi) = 0 \qquad (6)$$

where σ is the electrical conductivity of the analyte. With assumption that diffusion flux is small, the electrical conductivity is a function of the local ion concentrations and mobilities as follows:

$$\sigma = F\left(\sum_i c_i\left|\omega_{ep,i}\right| + \left|\omega_{ep,H}\right|[H^+] + \left|\omega_{ep,OH}\right|[OH^-]\right) \qquad (7)$$

Electric double layer

When an electric field is applied to a channel filled with electrolyte, an electric double layer (EDL) consisting of two parallel layers with opposite electrical charges forms along the channel surface which is responsible to the bulk movement of the fluid in that area. This layer is normally much thinner than the channel cross-sectional size and its description was not included in this model. Instead, its effect was represented by the electro-osmotic mobility (see Eqn.4) and a slip boundary condition applied for the channel walls.

ELECTROPHORETIC MOBILITIES OF IONS

The association/dissociation reactions of the salts are as follows:

$$KCl \leftrightarrow K^+ + Cl^-$$
$$NaCl \leftrightarrow Na^+ + Cl^-$$
$$LiCl \leftrightarrow Li^+ + Cl^-$$

Dissociation of above salts can be assumed to be complete and the resulted ions do not interact with water (neutral with respect to the solution pH). Dissociation of the buffer was taken into consideration. The dynamics of association/ dissociation reactions were ignored and the system was assumed to be at equilibrium. The mobilities of the ions and buffer solution are listed in Table 1.

Species	Mobility, $.10^{-9}$ m^2/(V.s)	pK_1	PK_2
K^+	76.2	-	
Na^+	51.9	-	
Li^+	40.1	-	
Cl^-	-79.1	-	
H^+	362.7	-	
OH^-	198.7	-	
MES	26.8	6.13	
Histidine	28.5	6.04	9.17

Table 1 Ion and buffer properties.

MEASUREMENT OF ZETA POTENTIAL OF THE CHANNEL WALLS

The electroosmotic mobility of the channel is required in both the experimental and computational modelling to account for the electrical double layer effect. It is directly linked to zeta potential of the channel walls via equation (4). There has been extensive experimental effort to quantify the zeta potential values for different substrates as reviewed by Kirby and Hasselbrink (2004a,b). While the glass and silica substrate data showed reasonable agreement among different research groups, the data for polymer substrate such as PMMA showed large uncertainties. This requires that specific measurement needs to be made for the chip used in the study.

The microfluidic chips were purchased from the Microfluidic ChipShop GmbH in Germany. A standard separation chip was used in the current experiments which was made of Polymethylmethylacrylate (PMMA). The chip has a simple T-channel (see Figure 1) and the length of the four channels measured from the cross to the center of the liquid ports is L1 = 6mm, L3 = L4 = 5mm, and L2 = 81.8 mm. The shape of the cross section of the channel is approximately rectangular with a height of 35 μm and a width of 70 μm. The chip is 95 mm long and 16 mm wide. The total thickness of the chip is 2 mm and the thickness of the cover lid for the channel is 30 μm. The PMMA material has a density of 1190 kg/m3.

All experiments were carried out in the CSIRO Microfluidics Laboratory at Highett, Melbourne, VIC 3190, Australia. The chip was used without treatment of the channel wall. Before experiments, the microchannel was cleaned with 0.1M sodium hydroxide (NaOH) for 10 minutes, then by deionized water rinse for 5 minutes followed by buffer solution for 30 minutes.

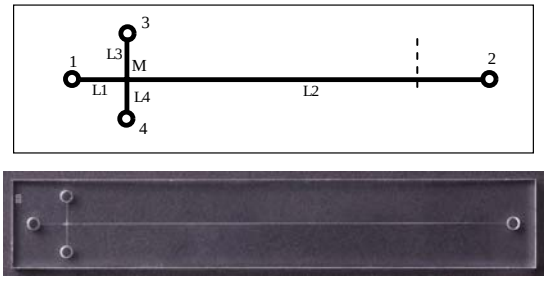

Figure 1 A diagram and a picture of the microfluidic chip. L1=6mm, L2=81.7mm, L3=L4=5mm. Measurement point (dashed line) was located at 14.7mm from port 2.

The Micralyne high voltage power supply system (Mycralyne, Edmonton, Canada) was used to control the

flow. The sample solution was injected from liquid port 3 to 4 for a period of 10 seconds at a voltage of 500V and then pushed into the separation channel at with an electrical potential of 2kV between ports 1 and 2. The voltage applied across terminals 1-2 and 3-4 is shown in Table 2.

Time, s	Applied voltage, V	
	1-2	3-4
0-10	0	500
10-150	2000	0

Table 2 Time-dependent applied voltage.

The solution used in all experiments was a MES/His buffer (20mM, pH of 6.1) with 50μM of KCl, NaCl and LiCl salts. All chemicals were purchased from Sigma-Aldrich and used without further purification. The DI water was obtained from the Milli-Q water purification system. Due to the low concentration of chemicals in the solution, the physical properties of the solution were assumed the same as those for DI water. The density of the solution is 1006 kg/m3, specific heat 4180 J/(kg.K), thermal conductivity k is 0.61, dynamic viscosity is $2.761 \times 10^{-6} \exp(1713/T)$ and dielectric constant is $305.7\exp(-T/219)$. The electrical conductivity of the buffer solution was assumed to be the same temperature dependence as that of water and with a room temperature value of 0.0494 S/m. The electrical conductivity and pH values at room temperatures were measured by a TPS SmartChem-CP system.

The electrophoretic mobility of the microchannel was measured using a current monitoring method (Huang et al., 1988). This experiment was performed using a slightly higher concentration buffer solution (22mM MES/His) to replace a 20 mM MES/His buffer. Electrical field applied was 2kV along separation channel. The current flowing through the microchannel increased as the higher concentration buffer solution entered the channel and the increase is linear. After the replacement was completed, the current was stabilised. The duration for the current change was obtained from the data and this allowed the electroosmotic flow velocity to be estimated. For the current separation conditions, this corresponds to an electroosmotic velocity of 0.323 mm/s. From the data in Table 1, the electrophoretic velocities were estimated to be 1.74, 1.18 and 0.91mm/s for the three ions K+, Na+ and Li+, respectively.

NUMERICAL METHODS

The above-described model was implemented based on the CFX-4 CFD software. The CFX-4 Algebraic Slip multiphase Model (ASM) was used to describe the movement of the ions. An extra equation of electrical potential distribution (6) was solved in parallel with the solution of the mass, momentum and species conservation equations. The high-order differencing schemes 'VAN-LEER' and 'SUPERBEE' were used for the momentum and species conservation equations, respectively, to minimize numerical diffusion. The flows at the inlets were assumed to be uniform with a magnitude same as the electroosmotic velocity. A slip boundary condition was used for the walls and the slip velocity was the same as the electroosmotic velocity $\omega_{eo} \nabla \phi$.

Simulations were conducted on a 1D and a 3D computational domains. The length of the 1D channel was 81.7 mm which corresponds to the length of the separation channel in the real microfluidic chip. The 3D domain included both sampling and separation channels with the correct channel cross section. However, only parts of these channels (near the sampling place) were present in this 3D domain. The applied voltages were scaled so that correct potential gradient was obtained along each channel.

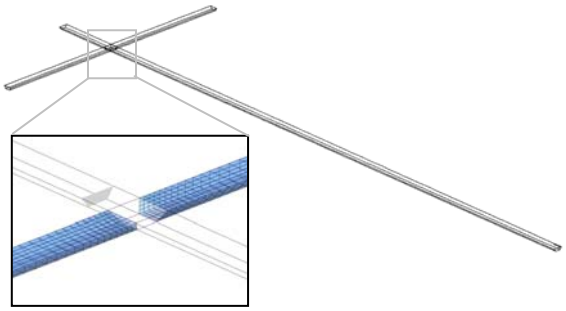

Figure 2 The 3-dimeniosnal computation domain**.**

RESULTS

3-D Simulations

The computational results for the 3D case are shown in Figures 3-5. The applied voltage was switched from terminals 3-4 to terminals 1-2 at 10s, which resulted in a short transition of the flow field as seen in Figures 3-4. The maximum velocity at the cross area was 0.75 mm/s and 0.34 mm/s before and after voltage switch, respectively. The value after voltage switch agreed well the estimated value of 0.323mm/s using experimental conditions, indicating that the flow was approximately slug-like. The slight variation in the cross area (more evident in Figure 4) was due to the boundary condition change, since near the cross area, there is no solid boundary.

Separation of the metal ions can be seen in Figure 5. For comparison, distribution of a neutral dye which was introduced into the domain together with the solution and passively followed the flow is shown in the figure. The effectiveness of electrophoretic motion is obvious due to the larger mobility of ions, as seen from the different locations of the neutral dye and the three ions at 2.5 s from the start of separation.

Figure 6 shows the iso-surface of dye concentration when the sample slug just entered the separation channel. It is clear that due to the transition of flow patterns from sampling to separation the sample concentration is non-uniform in the lateral directions. This is further enhanced by the non-rectangular shape of the channel cross-section. Such a non-uniformity caused significant dispersion of the sample ions as it travelled along the channel.

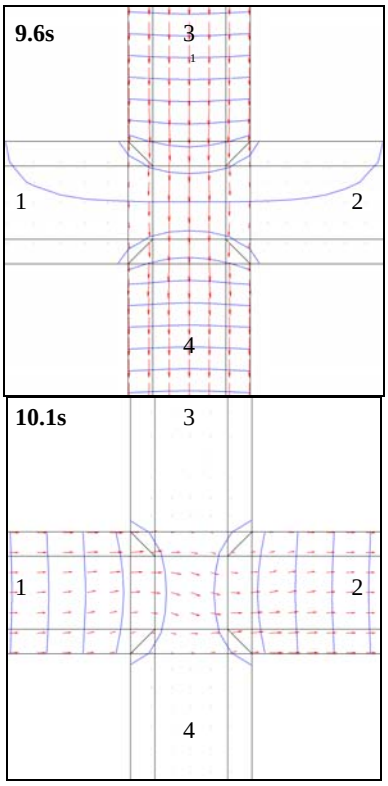

Figure 3 Contours of electrical potential and flow vectors at 9.6s and 10.1s.

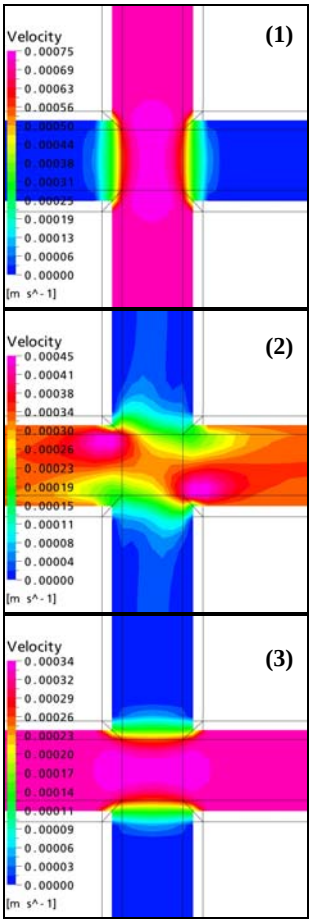

Figure 4. Transition of velocity at 9.6s (1), 10.1s (2), and 10.6s (3), when the voltage switched from 3-4 to 1-2.

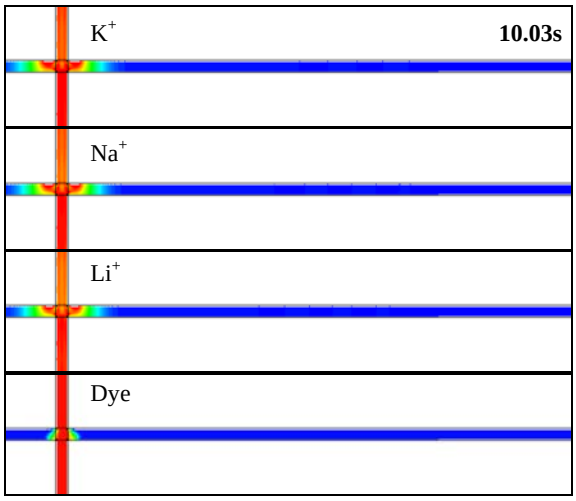

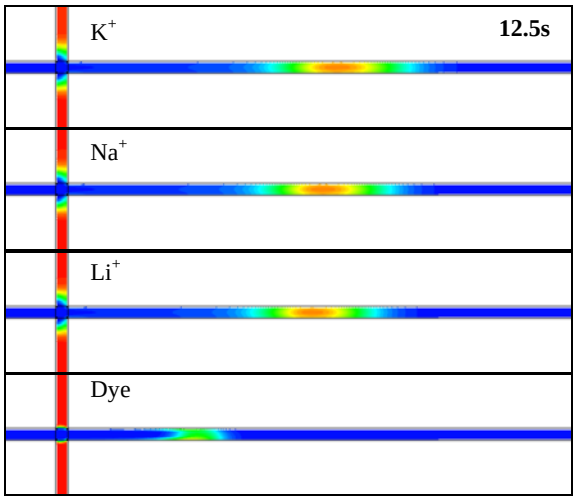

Figure 5 The computed distributions of the metal ions and dye at 10.03s and 12.5s.

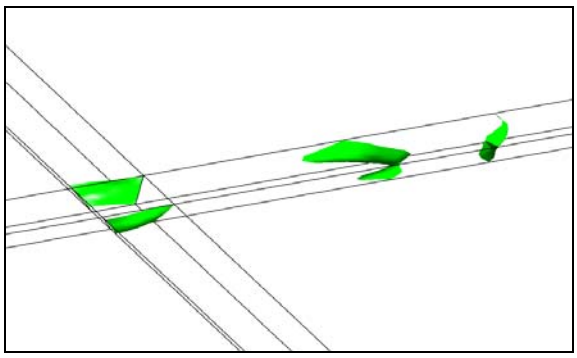

Figure 6 Iso-surfaces with the dye concentration equal 0.5 at 11s.

1-D Simulations

In the one-dimensional simulation, the full length of the separation channel was considered. The distributions of the metal ions K^+, Na^+ and Li^+ were initiated as equal square waves of 0.21 mm in length. Full separation of the metal ions is seen near the end of the 1D channel. Figure 7 shows the concentration profiles of the three ions along the channel at 35 s from the start of separation. The sequence of the three peaks and locations are consistent

with the mobility values of the three ions. For example, the potassium ion has a higher mobility value and thus travels faster. The effective velocity (i.e. the sum of electroosmosis velocity and electrophoretic velocity) is about 2.05mm/s and thus at a time of 35s, the peak will arrive at x = 72mm, as shown in Figure 7.

For a pure diffusion system, the spread of the concentration profiles can be estimated from Fick's second law of diffusion via

$$\frac{\partial c_i}{\partial t} = D_i \nabla^2 c_i \,. \qquad (8)$$

For a sample with an initial length $2L_0$ and concentration c_0, the concentration profile of i^{th} species is given analytically by

$$c_i(x,t) = \frac{c_0}{2}\left\{ erf\left(\frac{L_0 - x}{2\sqrt{D_i t}}\right) + erf\left(\frac{L_0 + x}{2\sqrt{D_i t}}\right)\right\}, \qquad (9)$$

where *erf* is the error function. The concentration profiles of the three ions at 35s from the start of the separation calculated using equation (10) are shown in

Figure 8. The differences in the numerically predicted and analytical concentration profiles (Figure 8 vs. Figure 9) are pronounced, reflecting that convective diffusion plays an important role. The initial sample concentration profile as well as the channel geometry and properties will affect the dispersion process and subsequently the separation efficiency. Therefore, a complete 3d simulation of the separation is required.

Comparison with measurements

The computed three peaks of the electrical conductivity which correspond to the passages of the K^+, Na^+ and Li^+ concentration waves through the measurement point are displayed in Figure 9. The arrival times of the three peaks were 35 s, 48 s and 58 s for K+, Na+ and Li+, respectively. These values agreed well with those estimated using the electrophoretic velocities of the three ions and electroosmotic velocity for the buffer solution. This is not surprising since the modelling used the estimated mobilities of the channel wall and ions. A more rigorous validation is by comparison with experimental data.

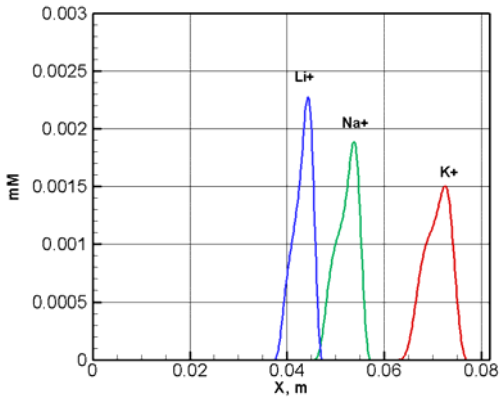

Figure 7 Molarities of K^+, Na^+ and Li^+ at 35s.

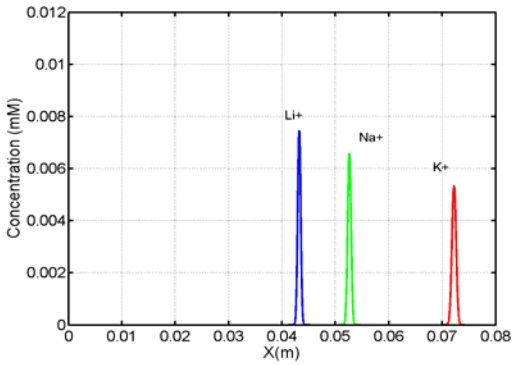

Figure 8 Calculated molarities of K^+, Na^+ and Li^+ at 35s assuming pure diffusion.

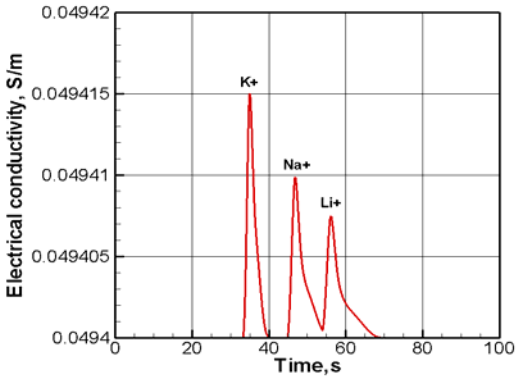

Figure 9 The computed electrical conductivity at the measurement point.

Figure 10 shows an electrophorogram of the three ions measured by a conductivity sensor attacked to the chip at a location of 72 mm from the intersection of the two channels. From the measurement, the arrival times were 42 s, 45 s and 58 s for K, Na and Li ions, respectively. The arrival times of Na and Li ions agree well (to within ±7%) the computational values. There is a relatively larger discrepancy (17%) between the measured and computed arrival time for K ion. However, the comparison between the modelled and measured data indicates that the computation model can reasonably predict the separation time for separation in microfluidic chip. The shape of the peaks, however, showed large difference due mainly to the simplified 1D model. Further work will be focused on a complete 3D modelling of the whole separation process.

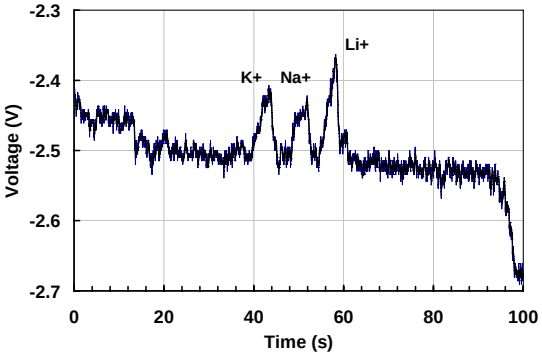

Figure 10 Measured electrophorogram for the three ions. Measurement location: 72mm from the intersection.

CONCLUSION

In this work, a model of the electrokinetically driven flow and electrophoretic separation of metal ions in a microfluidic chip was developed based on the generic CFX-4 CFD software. Important aspects of the involved electrochemical and physical processes were described through a set of the conservation equations and constitutive dependencies. The model was applied to investigate the flow and separation in a one-dimensional and three-dimensional domains with the latter correctly representing the channel geometry. Reasonable predictions of the flow and separation were obtained and the predictions were validated by measurements in terms of peak arrival time. The model can be used as a tool for design and optimization of the microfluidic separation chip.

REFERENCES

DOLNIK, V., LIU, S. and JOVANOVICH, S., (2000), "Capillary electrophoresis on microchip", *Electrophoresis*, **21**, 41-54.

ERMAKOV, S.V., BELLO, M.S., and RIGHETTI, P.G., (1994), "Numerical algorithms for capillary electrophoresis", *J. Chromatography A*, **661**, 265-278.

ERMAKOV, S.V., JACOBSON, S.C., and RAMSEY, J.M., (1998), "Computer simulations of electrokinetic transport in microfabricated channel structures", *Anal. Chem*., **70**, 4494-4504.

ERMAKOV, S.V., JACOBSON, S.C., and RAMSEY, J.M., (2000), "Computer simulations of Electrokinetic Injection techniques in microfluidic devices", *Anal. Chem*., **72**, 3512-3517.

HU, S., and DOVICHI, N.J., (2002), "Capillary Electrophoresis for the Analysis of Biopolymers", *Anal. Chem*., **74**, 2833-2850.

HUANG, X. M., GOTDON, J. and ZARE, R.N., (1988), "Current monitoring method for measuring the electroosmotic flow rate in capillary zone electrophoresis", *Anal Chem.*, **60**, 1837-1838.

IKUTA, N., and HIROKAWA, T., (1998), "Numerical simulation for capillary electrophoresis. I-Development of a simulation program with high numerical stability". *J. Chromatography A*, **802**, 49-57.

KIRBY, B. J. and E. F. HASSELBRINK JR., (2004), "Zeta potential of microfluidic substrates: 1. Theory, experimental techniques, and effects on separations", *Electrophoresis*, **25**, 187–202.

KIRBY, B. J. and E. F. HASSELBRINK JR., (2004) "Zeta potential of microfluidic substrates: 2. Data for polymers", *Electrophoresis*, **25**, 203–213.

KORYTA, J., DVORAK, J., and KAVAN, L., (1993), "Principles of Electrochemistry", 2nd Edition, John Willey & Sons.

PROBSTEIN, R. F., (2003), "Physicochemical hydrodynamics", 2nd edition, John Wiley and Sons.

SOUNART, T.L., and BAYGENTS, J.C., (2000), "Simulation of electrophoretic separations: Effect of numerical and molecular diffusion on pH calculations in poorly buffered systems", *Electrophoresis*, **21**, 2287-2295.

XUAN, X., XU, B., SINTON, D. and LI, D., (2004), Electroosmotic flow with Joule heating effects", *Lab Chip*. **4**, 230-236.

ZHU Y., S. NAHAVANDI, A. BUI, A. and K. PETKOVIC-DURAN, (2006), "Joule heating in a polymer microfluidic chip", *Proc. Of SPIE*, **6036**, BioMEMS and Nanotechnology II, paper no. 603612.

APPENDIX A – Dissociation constant of a realistic ionic system (Koryta et al. (1993))

Dissociation equilibrium constant for reaction

$$AB \leftrightarrow A^+ + B^-$$

is defined by

$$K = \frac{a_{A^+} a_{B^-}}{a_{AB}} = K' \frac{\gamma_{A^+} \gamma_{B^-}}{\gamma_{AB}},$$

where a is the component activity, γ is the activity coefficient, and

$$K' = \frac{[A^+][B^-]}{[AB]}$$

is the apparent or conditional dissociation constant based on the species concentrations at equilibria.

Degree of dissociation α or the fraction of the solution which dissociated at the given solute concentration is defined as

$$\alpha_{A^+} = \alpha_{B^-} = \frac{[A^+]}{[AB]+[A^+]} = \frac{[B^-]}{[AB]+[B^-]}.$$

This parameter is related to the apparent dissociation constant as follows (see Koryta et al., 1993)

$$\alpha = \frac{-K' + \sqrt{K'^2 + 4K'[AB]^0}}{2[AB]^0},$$

where $[AB]^0$ is the original concentration of solute AB.